Contents lists available at ScienceDirect

Environmental Research

Hallmarks of Alzheimer disease are evolving relentlessly in Metropolitan Mexico City infants, children and young adults. APOE4 carriers have higher suicide risk and higher odds of reaching NFT stage V at ≤ 40 years of age

Lilian Calderón-Garcidueñas[a,b,*], Angélica Gónzalez-Maciel[c], Rafael Reynoso-Robles[c], Ricardo Delgado-Chávez[b], Partha S. Mukherjee[d], Randy J. Kulesza[e], Ricardo Torres-Jardón[f], José Ávila-Ramírez[g], Rodolfo Villarreal-Ríos[h]

[a] *The University of Montana, Missoula, MT 59812, USA*
[b] *Universidad del Valle de México, 14370, Mexico*
[c] *Instituto Nacional de Pediatría, 04530, Mexico*
[d] *Mathematics Department, Boise State University, Boise, ID 83725, USA*
[e] *Auditory Research Center, Lake Erie College of Osteopathic Medicine, Erie, PA 16509, USA*
[f] *Centro de Ciencias de la Atmósfera, Universidad Nacional Autónoma de México, 04310, Mexico*
[g] *Grupo Médica Sur, Tlalpan 14050, Mexico*
[h] *Universidad Autónoma de Piedras Negras, Piedras Negras, Coahuila 26000, Mexico*

ARTICLE INFO

ABSTRACT

Exposures to fine particulate matter (PM$_{2.5}$) and ozone (O$_3$) above USEPA standards are associated with Alzheimer's disease (AD) risk. Metropolitan Mexico City (MMC) residents have life time exposures to PM$_{2.5}$ and O$_3$ above USEPA standards. We investigated AD intra and extracellular protein aggregates and ultrastructural neurovascular pathology in 203 MMC residents age 25.36 ± 9.23 y. Immunohistochemical methods were used to identify AT8 hyperphosphorilated tau (Htau) and 4G8 (amyloid β 17-24). Primary outcomes: staging of Htau and amyloid, per decade and cumulative PM$_{2.5}$ (CPM$_{2.5}$) above standard. Apolipoprotein E allele 4 (APOE4), age and cause of death were secondary outcomes.

Subcortical pretangle stage b was identified in an 11month old baby. Cortical tau pre-tangles, neurofibrillary tangles (NFT) Stages I-II, amyloid phases 1–2, Htau in substantia nigrae, auditory, oculomotor, trigeminal and autonomic systems were identified by the 2nd decade. Progression to NFT stages III-V was present in 24.8% of 30–40 y old subjects. APOE4 carriers have 4.92 times higher suicide odds (p = 0.0006), and 23.6 times higher odds of NFT V (p < 0.0001) v APOE4 non-carriers having similar CPM$_{2.5}$ exposure and age. Age (p = 0.0062) and CPM$_{2.5}$ (p = 0.0178) were significant for developing NFT V. Combustion-derived nanoparticles were associated with early and progressive damage to the neurovascular unit. Alzheimer's disease starting in the brainstem of young children and affecting 99.5% of young urbanites is a serious health crisis. Air pollution control should be prioritised. Childhood relentless Htau makes a fundamental target for neuroprotective interventions and the first two decades are critical. We recommend the concept of preclinical AD be revised and emphasize the need to define paediatric environmental, nutritional, metabolic and genetic risk factor interactions of paramount importance to prevent AD. AD evolving from childhood is threating the wellbeing of our children and future generations.

1. Introduction

Exposure to air pollutants plays a major role in the development and/or acceleration of Alzheimer's disease (AD) (Calderón-Garcidueñas et al., 2002, 2008; González-Maciel et al., 2017; Jung et al., 2015; Maher et al., 2016; Chen et al., 2017). Detrimental cognitive effects and brain metabolic and structural changes are described in the literature in healthy children (Calderón-Garcidueñas et al., 2011a, 2015a, 2015b, 2016a; Kicinski et al., 2015). Highly exposed Mexico City (MC) residents show an early brain imbalance in genes involved in oxidative stress, inflammation, and innate and adaptive immune responses (Calderón-Garcidueñas et al., 2012). Dysregulated neuroinflammation,

diffuse brain neurovascular unit damage, the accumulation of misfolded proteins associated to the early stages of both Alzheimer's and Parkinson's diseases are seen in MC youth and are absent in clean air controls (Calderón-Garcidueñas et al., 2008, 2012, 2010, 2016b, 2011b, 2017; González-Maciel et al., 2017).

Urban polluted environments and occupational exposures with ubiquitous distribution of high concentrations of ultrafine particulate matter (UFPM, nanosize particles < 100 nm) are of great concern for the central nervous system (CNS) due to the ease with which they penetrate biological barriers, including vascular endothelium, alveolar-capillary, olfactory, nasal, gastrointestinal, blood-brain-barrier (BBB) and blood-CSF barrier (González-Maciel et al., 2017; Maher et al., 2016; Calderón-Garcidueñas et al., 2016b, 2017).

Combustion-derived nanoparticles (CDNPs) are composed of iron and associated transition metals and are highly oxidative and strongly magnetic. Such particles can gain entry to the brain in significant amounts in young and older adult MC residents (Maher et al., 2016) and are known to cause severe damage to critical cellular organelles in the CNS in young urbanites (González-Maciel et al., 2017; Calderón-Garcidueñas et al., 2016b, 2017).

We have one primary aim for this study: To document in young urbanites by immunohistochemistry the early stages of the pathological process in Alzheimer disease (Braak and Del Tredici, 2011, 2015; Braak et al., 2011; Thal et al., 2002; Rüb et al., 2016). We are concerned about the disease progression with age and cumulative exposures to fine particulate matter (PM$_{2.5}$) above the USEPA standard. Given that the neurovascular unit (NVU) plays a key role in maintaining an equilibrated coupling between neural activity and blood flow, and failure is part of the AD developing process, we documented by electron microscopy NVU changes in childhood and teen years (Iadecola, 2017).

The early identification of AD in air pollution highly exposed young individuals and understanding the mechanistic pathways involved, are at the core of our research efforts. Identifying key air pollutants impacting neural risk trajectories would greatly facilitate multi-disciplinary prevention efforts for potentially modifying the course of AD in paediatric and young adult ages.

2. Methods

2.1. Air quality data

Mexico City residents are exposed year-round to fine particulate matter (PM$_{2.5}$) and ozone (O$_3$) concentrations above the United States National Air Ambient Quality Standards (NAAQS). For this study, we focused on < 2.5 μm particles and work with cumulative PM$_{2.5}$ (CPM$_{2.5}$) above the annual USEPA standard: 12 μg/m^3, reflecting lifetime exposures above the standard. Both, the PM$_{2.5}$ annual standard and the 24-h 35 μg/m^3 standard have been historically exceeded across the metropolitan area for the last 20 years (Bravo-Alvarez and Torres-Jardón, 2002; Vega et al., 2010; SEDEMA, 2017).

The accumulated burden of PM$_{2.5}$ for each subject-included pregnancy-was calculated based on their urban residency. Historical PM$_{2.5}$ levels were obtained from a combination of particulate matter data from Mexico City Government Manual Monitoring Network for five representative urban sites: Tlalnepantla (NW), Xalostoc (NE), Pedregal (SW), Iztapalapa (SE) and Merced (downtown) (Fig. 1) and an approach considering the typical PM$_{2.5}$/PM$_{10}$ ratio for each of the representative sites. The highest PM$_{2.5}$ concentrations occur in the NE sector where industrial and traffic activities are prevalent, and decrease towards the SW residential area. We selected to work with a cumulative PM$_{2.5}$ (CPM$_{2.5}$) exposure based on the assumption that long-term concentrations above the annual, averaged over 3 years USEPA standard of 12 μg/m^3 standard, would have detrimental health effects. To estimate theCPM$_{2.5}$ we used the expression:

$$CPM_{2.5} = \sum \max([\text{annual mean PM}_{2.5}] - 12\,\mu g/m^3, 0)\Delta t$$

where the "max" function ensures only annual mean PM$_{2.5}$ values are included. The backward summation was taken over the life time age (Δt) of each subject back to their prenatal period. The procedure was based on the assumption that the trend of PM$_{2.5}$/PM$_{10}$ ratio obtained from the slopes of the correlations of these species in the period 2004–2010 represent the backward PM$_{2.5}$/PM$_{10}$ ratios trends for previous years. The results compared well with a number of PM$_{2.5}$/PM$_{10}$ ratios reported by academic groups in conference proceedings and published papers related to PM pollution in Mexico City in the 1980–1990 years (Bravo-Alvarez and Torres-Jardón, 2002; Vega et al., 2010). The resulting ratios were then used to estimate the PM$_{2.5}$ annual averages for each of the selected sites for the period 1989–2003. Since the study population included individuals older than 30 years at their time of death, we assumed a constant value for the PM$_{2.5}$ annual averages prior to 1989 equal to the annual mean for this year. Overall, the PM$_{2.5}$/PM$_{10}$ ratios were relatively constant ranging from ~ 0.45 in the southwest towards ~ 0.25 in the northeast. High PM$_{2.5}$/PM$_{10}$ ratios indicate a dominance of coarse particles in the PM$_{10}$ while low ratios are associated to prevalence of fine particles.

With the estimated PM$_{2.5}$ annual averages for each site and year, we obtained a working annual average by averaging the 3 previous consecutive years according with the procedure to calculate the USEPA annual mean standard, moving backwards in time up to 30 years. The resulting working annual average was used to obtain the CPM$_{2.5}$ with our equation for each of the individuals in the study, starting 1 year before their year of birth and up to the age of death (Table 1, Suppl). The working average data base was chosen according with the closest sampling site to their residence addresses during most of their life.

Chemical PM composition studies in Mexico City have shown that the proportion of the different component PM species has not changed significantly along the years (Bravo-Alvarez and Torres-Jardón, 2002; Vega et al., 2010; Molina et al., 2010; Aiken et al., 2009) The PM$_{2.5}$/PM$_{10}$ ratio variations and the PM chemical composition are dependent on the site location and on the season. Typically, the coarse PM in MC is strongly dominated by geological material (SiO$_2$ + CO$_2^{-3}$ + Al$_2$O$_3$ + Ca + Fe + Mg + K) from dust resuspension. Organic and carbonaceous aerosols are the dominant species in the PM fine fraction. Particle emissions from gasoline and Liquefied Petroleum Gas Combustion (LPG) are dominated by organic carbonaceous aerosols (OC), while in diesel particles, black carbon (BC) is the main component (Molina et al., 2010). Organic aerosols in the air include primary hydrocarbon-like compounds, oxygenated organic compounds mostly secondary, organics from biomass burning, and small contributions of nitrogen-containing organics of primary combustion (Aiken et al., 2009). Also, critical for the brain effects, BC concentrations in PM$_{2.5}$ have not shown a decrease through the years (Aiken et al., 2009). BC is associated with polycyclic aromatic compounds (PAHs), semi-volatile species resulting from incomplete combustion of carbonaceous fuels such as gasoline and diesel vehicle exhaust gases (Marr et al., 2006). Most of PAHs in MMC are present in PM$_{2.5}$. Trace metals in fine particles include Zn, Cu, Pb, Ti, Sn, Ba, Mn, Sb, V, Se, As, Ni, Cd, Cr in that order (Querol et al., 2008). Zn, Cu, Ba, Pb and Cd are tracers of road traffic, while V and Ni are tracers of industrial emissions. Exposures to ozone concentrations are also above the USEPA standards (annual fourth-highest daily maximum 8-h concentration, averaged over 3 years) all year long (Fig. 1). All other criteria pollutants for MMC, including nitrogen dioxide, sulfur dioxide and lead have shown elevated levels prior to 2000, but have been at or below the current USEPA standards in the last 17 years (Secretaría del Medio Ambiente del Distrito Federal).

2.2. Study design and samples

Two hundred and three consecutive autopsies with sudden causes of death, not involving the brain were selected for this study. MMC subjects age 11 months to 40 years were clinically healthy prior to their sudden demise and were included in the study if macro and microscopic
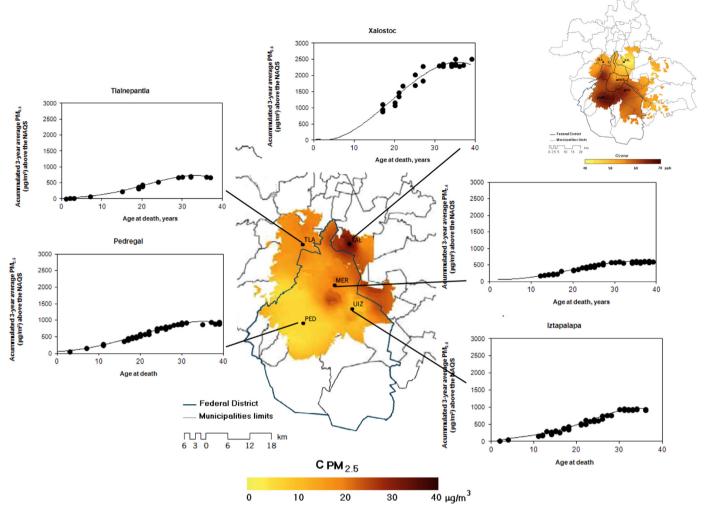
Fig. 1. Cumulated PM$_{2.5}$ trends of the annual, averaged over 3 years, mean concentrations in excess the USEPA standard for 203 individuals according to their age at the time of death and residential location. The regressions are overlapped on a map showing the spatial distribution of the annual PM$_{2.5}$ concentrations for the base year 2008 (the last year of the 5 y study). The map in the upper right corner shows the spatial distribution of the annual average of the daily ozone 8-h maximum for 2008.

examination of extra-neural key organs was unremarkable, and if gross examination of the brain was unremarkable. Specifically, we ruled-out cases with orbital lesions, cortical atrophy, evidence of recent or old infarcts, brainstem abnormalities and ventricular enlargement. Examination of autopsy materials was approved by the Forensic Institute in Mexico City. Autopsies were performed 4.1 ± 1.7 h after death between 2004 and 2008, and samples were collected by 4 trained researchers, weekdays, weekends and holidays during the 5 year study period. Brains were examined macroscopically, sections were selected for light and electron microscopy, and frozen tissues collected for genotyping. The general characteristics of the study population, including their cause of death are seen in Table 1 (Suppl). The selected brain sections included a minimum of six blocks: superior and middle frontal cortices (Brodmann Areas 9/46), midduncal level through medial temporal lobe including hippocampal formation, parahippocampal gyrus and transentorhinal region, inferior parietal lobule, olfactory bulb, caudate and putamen. Brainstems were sectioned from the midbrain at the level of the superior colliculi to the lower medulla. An average of 10.7 ± 4.18 blocks was obtained from each brainstem and 76 ± 13 slides were examined per block. Paraffin embedded tissue was sectioned at a thickness of 7 μm and stained with hematoxylin and eosin (HE). Immunohistochemistry (IHC) was performed on serial sections as previously described (Calderón-Garcidueñas et al., 2008). Antibodies included: β amyloid 17-24, 4G8 (Covance, Emeryville, CA 1: 1500), PHF-tau8 (Innogenetics, Belgium, AT-8 1:1000). Brain tissues were

blindly investigated for purposes of AD staging by Board certified neuropathologists and anatomical pathologists. Early subcortical lesions and early cortical lesions as described by professors Braak and Del Tredici (2011, 2015), Braak et al. (2011), the amyloid-β protein phases (Thal et al., 2002) and the brainstem tau pathology (Rüb et al., 2016) were the focus of this work. Prefrontal and olfactory bulb tissue blocks were processed for EM (González-Maciel et al., 2017) with a focus on the neurovascular unit and the presence of CDNPs. Genotyping for the presence of APOE alleles and the Asp299Gly Toll-like receptor-4 (TLR-4) polymorphisms was done as previously described (González-Maciel et al., 2017; Calderón-Garcidueñas et al., 2015b, 2016a, 2012; Kicinski et al., 2015).

2.3. Statistical analysis

Our sample size of 203 subjects was defined a priori by sampling logistics in the 5 year study period and balancing the expected results from previous neuropathology studies in young urbanites (Calderón-Garcidueñas et al., 2008, 2012, 2010, 2016b, 2011b, 2017; González-Maciel et al., 2017). We focused on summary statistics and graphical summary of the concerned staging variables: the two major markers of Alzheimer's disease Htau and amyloid- β, and age, gender, mode of death, and APOE status. Mode of death was analyzed in three major groups: accidents, homicides, and suicides. We identified APOE4 carriers as individuals with higher risk of suicide, and we performed a

goodness of fit test to check if the percentages of APOE4 in the suicide group and in the other groups involving accident and homicide were the same. We performed logistic regression analyses to model the odds of committing suicide with relevant predictors including age, cumulative $PM_{2.5}$, and APOE status and, also to model the odds of developing NFT stage V with the same predictors. We calculated cumulative incidence probabilities of committing suicide with $CPM_{2.5}$ among APOE4 non-carriers and APOE4 subjects after adjusting the subjects' age. We also calculated cumulative incidence probabilities of developing various stages of Htau pathology with $CPM_{2.5}$. Finally, we plotted those probabilities. We performed the statistical analyses using Excel and the statistical software 'R' (http://www.r-project.org/).

3. Results

Fig. 1 and Table 1 (Suppl) show the annual mean averages of $CPM_{2.5}$ for each individual based on their residence within arbitrary centroids in each of the five selected sampling sites. A polynomial regression of second degree was applied to the $CPM_{2.5}$ data for each site. The regressions were overlapped on a figure of the estimated spatial distribution of the annual average $PM_{2.5}$ concentrations in MMC for 2008. In Fig. 1, the insert figure shows the annual average of the daily ozone 8-h maximum for the same year. Htau and amyloid-β staging per cause of death and APOE4 are seen in Fig. 2. Having an APOE4 allele significantly increased the odds for developing NFT V (p < 0.0001), and it was about 23.6 times the corresponding odds for APOE4 non-carriers, at the same age and having the same $CPM_{2.5}$ exposures. Fig. 3 shows the distribution of Htau and amyloid-β stages by decade. Both age (p = 0.0062) and $CPM_{2.5}$ (0.0178) are significant predictors for modelling the odds of developing NFT Stage V by logistic regression. In a model where $CPM_{2.5}$, age and APOE status were included as suicide predictors, having an APOE4 significantly increases the odds of dying by suicide (p = 0.0006), and increased 4.92 times the corresponding odds v APOE4 non-carriers having similar $CPM_{2.5}$ exposures and age
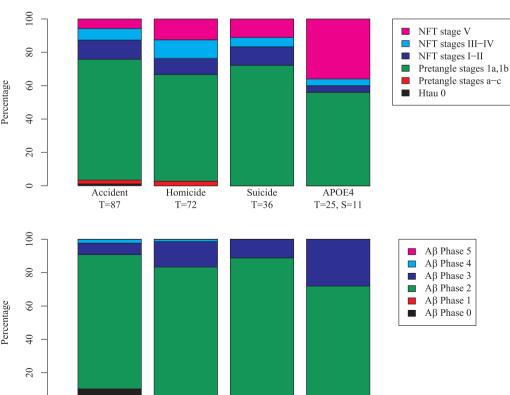
(Fig. 4).

Development of Htau pretangle stages is associated with $CPM_{2.5}$ in an average range of 900 μg/m³, while development of NFT stages is associated with much higher amounts of $CPM_{2.5}$ (Fig. 5). The 12.3% distribution of APOE4 in the working cohort was significantly different from the open MMC population distribution, of 18.7% (Calderon's laboratory data). The Chi-squared test with Yates' continuity correction gave two-sided p-value = 0.0051 (χ^2 = 7.8475, d.f. = (2 − 1) × (2 − 1) = 1) showing that the percentage of APOE4 in the suicide group (30.6%) is indeed significantly higher than combined accident and homicide groups (8.4%). We had one 22 y old female APOE 3/3, dying in a car accident as a passenger, with a TLR 4 Asp299Gly polymorphism associated with a blunted response to inhaled lipopolysaccharides. AD markers yield negative results in this young woman.

3.1. Neuropathology

The brains of 203 individuals staged for AD pathology could be classified (Braak and Del Tredici, 2011, 2015; Braak et al., 2011; Thal et al., 2002; Rüb et al., 2016). Htau neurites in brainstem sections (involving the reticular formation, vagal and trigeminal nuclei), diffuse amyloid cortical plaques and abnormal neurovascular units characterized children ≤ 7 y (n: 8) (Fig. 6), while children and young adults 11–20 years old (n: 61) all showed progressively more Htau brainstem involvement, along with cortical tangles and amyloid plaques (Figs. 7 and 8). Nuclear Htau was identified in neurons, glia and endothelium throughout the brain.

3.2. First decade findings

Children ≤ 10 y (n: 8) all showed positive Htau neurites in their medulla (Fig. 9). Htau location in the lower medulla sections included the reticular formation (lateral, medial and raphe nucleus), dorsal motor neuron of the vagus (X) and spinal trigeminal nerve (V). All eight

Fig. 2. Percentages of H-tau stages and Amyloid-β phases among subjects dying of external causes of death and subjects having an APOE4 allele. T = total number of subjects in the corresponding group, S = number of deaths by suicide Percentage = percentage of subjects with specific Htau stage or Aβ phase in the corresponding group. In the APOE4 group, all subjects carrying an allele 4 were included irrespective of their mode of death.
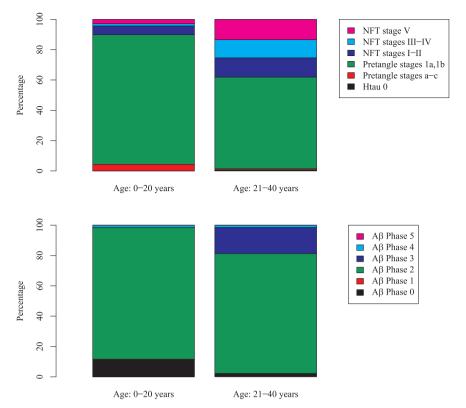
Fig. 3. Percentages of H-tau stages and Amyloid-β phases by age: 0–20 and 21–40 years at the time of death. Percentage = percentage of subjects having relevant Htau stage or Aβ Phase in the corresponding age group. We included all subjects regardless of cause of death. T = the number of subjects in the corresponding group.

children were APOE 3/3 and all were classified as pretangle stages a–c, 1a, 1b. Abnormal neurovascular units were noted (Fig. 10) and isolated beta pleaded sheet helicoidal conformation fibers were observed in pericytes along with CDNPs of sizes ranging from 28 to 60 nm.

3.3. Second decade findings

The location of Htau neurites, cytoplasmic Htau and tangles in children and teens between 11 and 20 years of age included: the central and periaqueductal gray, medial longitudinal fasciculus, gigantocellular reticular nucleus, dorsal motor vagal and solitary nuclei, intermediate reticular zone, reticulotegmental nucleus of pons, medial lemniscus, trigeminal-thalamic ventral tract, nucleus ambiguous, pars compacta of the substantia nigrae, pedunculopontine nucleus, spinal trigeminal nucleus, locus coeruleus, inferior colliculus, dorsal cochlear and vestibular nuclei. One globose Htau positive tangle in the brainstem were seen in a 13 y old girl (Fig. 7H). One micron toluidine blue sections show the extensive damage to the neurovascular unit (Fig. 11A–C). Changes in basement membranes (BM) with thickening and deposition of abnormal BM layers were particularly prominent in the olfactory bulb (Fig. 11D). Vascular and neuropil beta pleaded sheet helicoidal conformation fibers were seen, lipofuscin was abundant, and CDNPs across endothelial BMs and in myelinated frontal axons were common (Fig. 11E–H). CDNPs were seen in axonal mitochondria, in close contact with neurofilaments and myelin sheets and in choroid plexus epithelium with a range size of 8–66 nm in diameter (Fig. 11H, I).

3.4. Third and fourth decade findings

Progression to NFT stages III–V was present in 24.8% of 30–40 y old subjects. Bielschowsky's silver stain positive neurons and Htau cytopathology, were evident by the 3rd and 4th decades (Fig. 12A–K). Locus coeruleus sections were examined in 117 cases and 35.89% (n: 42) showed Htau pathology (Fig. 12A), while 54% showed various degrees

of degranulation of pigmented neurons. Amyloid plaques and vascular pathology were prominent and cytoplasmic neuronal amyloid accumulation was a common finding (Fig. 12G, H, L).

4. Discussion

The presence of cerebral tau pathology and extracellular aggregated amyloid-β in 202/203 consecutive young brains constitute a serious health crisis. Metropolitan Mexico City has one of the highest levels of traffic air pollution in the world, its residents being exposed from conception to concentrations of PM$_{2.5}$ and O$_3$ above USEPA standards (Calderón-Garcidueñas et al., 2008, 2016a, 2017; González-Maciel et al., 2017). Highly oxidative and ubiquitous combustion-derived nanoparticles (CDNPs) are associated with early and progressive damage to the neurovascular unit, supporting they are likely suspects for cell damage and neurotoxicity (González-Maciel et al., 2017; Maher et al., 2016; Calderón-Garcidueñas et al., 2016b, 2017; Yarjanli et al., 2017). The finding of early extensive nuclear neuronal Htau strongly supports a cerebral stress response previously documented by upregulation of clusters of IL1, NFκB, TNF, IFN, and TLRs and a 15-fold frontal downregulation of the prion-related protein, severely compromising oxidative stress protection (Calderón-Garcidueñas et al., 2012). Sultan et al. (2011) suggested nuclear tau is a key player in early stress responses and stated, *"pathological alterations of Tau, e.g., hyperphosphorilation, might impair its ability to shuttle between the cytoplasm and the nucleus and/or affect its affinity for DNA".* Thus, the extensive nuclear Htau would fail to efficiently protect DNA from oxidative stress damage and as emphasized by Sultan et al. (2011) *contribute to functional failure of neurons* early in life.

The speed of disease progression is given by the presence of an APOE4 allele, age, and CPM$_{2.5}$. APOE4 increased the odds for developing NFT V, and strikingly it was 23.6 times the corresponding odds for APOE4 non-carriers, with similar age and CPM$_{2.5}$ exposures. Age and CPM$_{2.5}$ are also significant for modelling the odds of developing
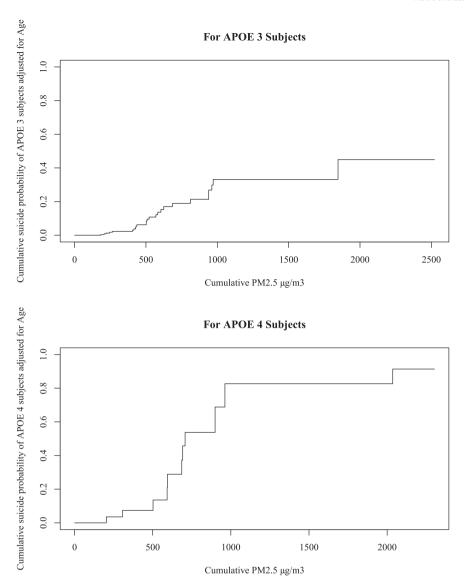
For APOE 3 Subjects

For APOE 4 Subjects

Fig. 4. Cumulative suicide probability among subjects carrying APOE3 and APOE4 alleles as a function of cumulative PM$_{2.5}$ exposures, after adjusting for age. We used Cox's proportional hazard model to estimate the underlying survival function and used the subject's age as a predictor.

NFT Stage V. These data being very relevant for highly exposed city dwellers, occupational exposures and exposures to natural disasters (i.e., forest fires), given that Braak and Del Tredeci (2015) have suggested, and we fully agreed "*continual formation of abnormal tau takes place from the beginning until the end-phase of Alzheimer's disease and is not known to be subject to remission*". In sharp contrast with results in Braak et al. (2011) 2332 autopsies ages 0–100 years, where amyloid-β plaques began to appear between ages 30 and 40, at the time subjects exhibited pretangle stage 1a or 1b, in our cohort, diffuse amyloid plaques are seen at age 11 months, and by the time children/ teens reach pretangle stage 1a or 1b they also have amyloid-β phase 2.

Indeed, we are witnessing an accelerated Alzheimer disease process with striking time lines, and disease progression pace. We strongly suggest the first two decades of life are critical for brain damage associated to environmental pollutant exposures, and although there is no doubt considerable individual AD progression differences are likely determined by APOE and factors such as gender, metabolism, nutrition, genetics, occupational history and others (Calderón-Garcidueñas et al., 2008, 2015a, 2015b, 2016a, 2012, 2017; González-Maciel et al., 2017) the persistence and progression of Htau lesions in young children, based on classic neuropathology studies (Braak and Del Tredici, 2011, 2015; Braak et al., 2011; Thal et al., 2002; Rüb et al., 2016), ought to

represent a serious short and long term health problem. The presence of Htau positive globose tangles in the brainstem of 13 year olds, raises the question of other evolving tauopathies (Kovacs, 2017).

Most researchers are focused on the development of mild cognitive and behavioral impairment and clinical symptoms associated with late AD stages and a preclinical phase in which AD neuropathology begins to accumulate but cognitive performance is normal (Sperling et al., 2011).

Mexico City children have a short *silent stage and Htau is the key abnormal protein to cause early symptoms*. In our clinical studies of healthy children ≥ 6 years, carefully screened MC v clean air controls, matched by age, gender, socioeconomic status and mother's IQ, have already clinical, cognitive, olfactory, auditory, CSF and brain MRI/MRS alterations in the absence of risk factors, other than their environmental exposures to air pollutants (Calderón-Garcidueñas et al., 2011a, 2015a, 2015b, 2016a, 2010, 2011b). APOE modulates the group effects between WISC-R and left frontal and parietal white matter, and hippocampus metabolites. Olfaction is affected in the preteen years, soap is the predominantly failed odor, and in APOE4 carriers, strongly correlated with left hippocampus mI/Cr ratio (Calderón-Garcidueñas et al., 2015a). In a cohort of children and their parents ages 12.45 ± 3.4 and 37.5 ± 6.78 years, the right hippocampus NAA/Cr
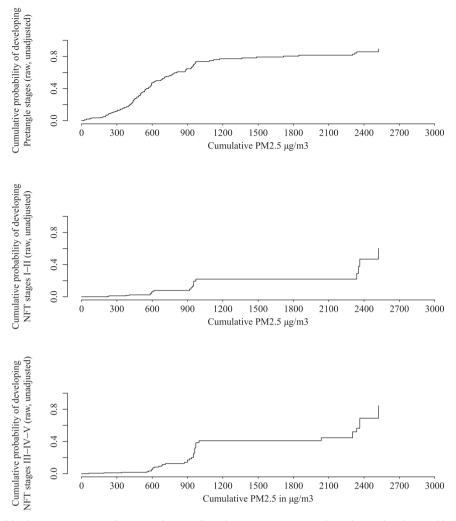
Fig. 5. Cumulative probability of developing various stages of H-tau as a function of cumulative PM$_{2.5}$ exposures without adjusting for other possible predictors. We used Kaplan-Mier method to estimate the underlying survival function.

ratio was significantly lower in MC subjects, potentially reflecting neuronal density, and loss of synapses associated with higher Htau burden (Calderón-Garcidueñas et al., 2015b). Strikingly, APOE4 heterozygous MC females age 12.3 ± 5.4 years, with > 75% to < 94% BMI percentiles are at the highest risk of severe cognitive deficits (1.5–2 SD from average IQ) (Calderón-Garcidueñas et al., 2016a). We have also shown in normal CSF samples, Aβ1-42 and Brain Derived Neurotrophic Factor concentrations are significantly lower in MC v controls (p = 0.005 and 0.02, respectively) and macrophage inhibitory factor, a key neuro-immune mediator is significantly higher in exposed children (Calderón-Garcidueñas et al., 2016c). The low CSF Aβ1-42 concentrations (with normal total tau and tau phosphorylated at threonine 181) in MC children age 11.2 ± 5.5 years are likely in keeping with predominantly Phase 2 amyloid seen in the first two decades and the accumulation of amyloid in choroid plexus (CP) epithelium loaded with CDNPs at preteen and teen ages (Fig. 7S). Since CP failure is described in AD, it will be imperative to study CP function impact in early AD pathogenesis.

The lower brainstem involvement deserves a comment. It is the earliest tau cytoskeletal pathology site in our children and the target nuclei affected are likely pointing towards key portals of entry: the nasal mucosa through trigeminal mucosal afferents and tracheal and gastrointestinal mucosa through vagal afferent terminals. We have shown in 24.0 ± 10.5 y cohorts, the presence of Htau in gastric and vagus nerve (cervical level) samples, thus is important to know AD pathology in these highly exposed subjects is not confined to the brain

(Calderón-Garcidueñas et al., 2017). CDNPs are penetrating and damaging the GI barrier thorough the small intestine and stomach and reaching the vagus (Calderón-Garcidueñas et al., 2017). Clinical involvement of the auditory system, results in delayed central conduction time of brainstem neural transmission in children age 8.0 ± 0.7 y v controls (Calderón-Garcidueñas et al., 2011b). Also, worth commenting, is the involvement of the substantia nigrae by Htau neurites, tangles, and plaques and various degrees of extraneuronal neuromelanin being phagocytosed by microglia. Nuclear Htau is observed in satellite glia of pars compacta neurons at age 11 months, is strikingly present in the cytoplasm of endothelial cells in small capillaries in the midbrain at age 2 years, while a decade later the number of Htau neurites in the pars compacta has increased significantly, strong nuclear Htau is present in neurons and pigmentary incontinence in phagocytic cells is common. Neuromelanin interacts with inorganic and organic compounds and avidly binds iron and heavy metals aimed to reduce their toxicity (Zecca et al., 1969). Its high capacity storage trapping system for metal ions could be overcome by interaction with strongly magnetic nanoparticles of magnetite (mixed Fe^{2+}/Fe^{3+} iron oxide) often associated with transition metals (Maher et al., 2016). These combustion NPs abundant in MC brains and present in the abnormal neurovascular units in the brain could be easily transferred from red blood cells to endothelial cells to substantia nigrae cells and cause extensive damage to mitochondria, endoplasmic reticulum (ER), mitochondria-ER contacts (MERCs), axons and dendrites (González-Maciel et al., 2017).
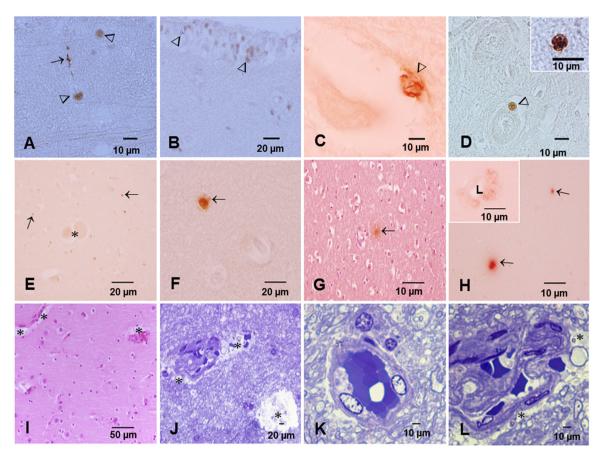
Fig. 6. Representative immunohistochemistry (IHC), one micron toluidine blue and H&E sections from children in the first decade of life. A. Eleven month old APOE 3/3 with a hyperphosphorilated tau positive neurite in the mesencephalic reticular formation. Numerous nuclei are Htau + . IHCxAT8. Scale bar 10 µm. B. Same child a A. Ependymal multiciliated cells around the cerebral aqueduct show positive nuclear Htau. IHCxAT8. Scale bar 20 µm. C. Same child as A and B. Substantia nigrae neuron with positive Htau in neuronal hillock. IHCxAT8. Scale bar 10 µm. D. Three year old APOE 3/3. Substantia nigrae neurons show perineuronal glial cells with strong nuclear Htau staining. INSERT. In the same area, a glial cell with strong nuclear Htau staining shows a filamentous Htau extension. Scale bar 10 µm. E. Same 3 year old as D. Periventricular gray with numerous cells with Htau positive nuclei. Mesencephalic V neurons marked with an (*) IHCxAT8 Scale bar 20 µm. F. Eleven month old, frontal section. Neuron with Htau strongly positive nuclear staining. IHCxAT8 Scale bar 20 µm. G. Eleven month old, frontal section with a diffuse amyloid plaque. IHCx4G8 Counterstained with hematoxylin. Scale bar 10 µm. H. Seven year old girl, temporal section with two diffuse amyloid plaques. IHCx4G8. Insert: temporal blood vessel with positive endothelial cells cytoplasmic amyloid-β, lumen marked L. IHCx4G8 Scale bar 10 µm. I. Two year old male APOE 3/3 frontal section. The mild enlargement of the Virchow-Robin spaces (*) is the only remarkable finding by light microscopy. H&E Scale bar 50 µm. J. Three year old boy, 1 µm toluidine blue section of temporal lobe white matter. The enlargement of the Virchow-Robin spaces is marked by (*). Cell, myelin and red blood cell fragments in enlarged Virchow-Robin spaces (*) characterize the white matter in temporal section 1 µm Toluidine blue. Scale bar 20 µm. K. Higher power of small arteriole in temporal white matter (same child as J). Endothelial cells with prominent cytoplasm and enlarged Virchow-Robin spaces with rarefaction of the adjacent neuropil and variation in the size of myelinated axons (*). 1 µm Toluidine blue. Scale bar 10 µm. L. A larger convoluted arteriole shows an expanded Virchow-Robin space with cell fragments and fragmented axons (*). 1 µm Toluidine blue. Scale bar 10 µm.

The extensive and progressive damage to the neurovascular unit (NVU) – the anatomical substrate of neurovascular interactions – (Iadecola, 2017) is a critical finding in the setting of a developing AD process in young subjects. Failure in its most vital role: *the coupling between neural activity and blood flow* (Iadecola, 2017), will result in neurovascular dysfunction-as in AD-, failure in orchestrating neuronal-astrocytic signaling to local blood vessels and the release of mediators across the cerebrovascular network (Iadecola, 2017). A damaged NVU-thickness, splitting and duplication of the basement membranes, abnormal tight junctions and mitochondria in endothelial cells (ECs), and pericytes, and amyloid-β accumulation (González-Maciel et al., 2017) will allow direct exposure of the brain to neurotoxins, pathogens and harmful chemicals. NVU damage in MMC children and young adults is at the core of AD pathology with all the resultant hypoxia and neurovascular impairments during disease progression (Calderón-Garcidueñas et al., 2016b).

Based in our brainstem findings, we fully support Braak and Del Tredeci (2011) stating "*is precisely during the first decades of life that the probability of encountering brainstem AD-associated intraneuronal lesions without involvement of cortical predilection sites is high*" and we argue trigeminal and vagal nerves are likely key portals of entry for a direct hit to brainstem nuclei (Rüb et al., 2016). We also fully agreed

with Braak and Del Tredeci (2015) that *a trigger for tau protein hyperphosphorilation and conformational change* ought to be at work, but we strongly support combustion-derived nanoparticles and NPs of other sources, are the culprit (González-Maciel et al., 2017). CDNPs in close contact with neurofilaments, glial fibers, and chromatin are seen in MMC children, and they are certainly potential sources for altered microtubule dynamics, mitochondrial dysfunction, and accumulation and aggregation of unfolded proteins including tau, β-amyloid and α-synuclein (González-Maciel et al., 2017; Maher et al., 2016; Calderón-Garcidueñas et al., 2017). Indeed, iron oxide NPs can produce iron accumulation, oxidative stress and protein aggregation in neural cells (Yarjanli et al., 2017). The conformational abnormal tau could be the result of the direct interaction with NPs and since the NPs have anterograde, retrograde axonal and trans-synaptic trafficking capabilities and can be transported directly to the brain through the nose and the GI tract, NPs could be strong candidates for the *tau protein hyperphosphorilation and conformational change* of β-amyloid and α-synuclein (Yarjanli et al., 2017; Alvarez et al., 2013). Basic nanoparticles characteristics such as size, shape, surface charge, surface chemistry, chemical composition, surface coating, solubility, mode of entry, biocorona composition, competition for site receptors, targeted organelles, and cell type will be determining cytotoxicity, genotoxicity, and the
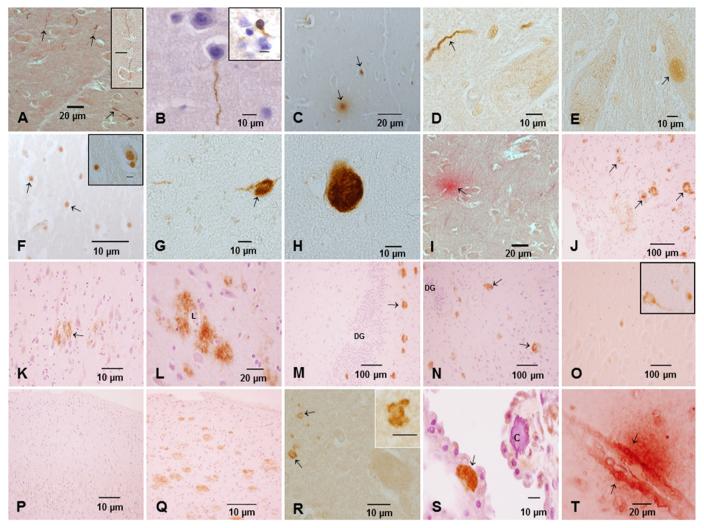
Fig. 7. Representative immunohistochemistry and one micron toluidine blue and H&E sections from subjects in the second decade of life. A. Eighteen year old male, APOE 3/4 frontal section. Numerous Htau neurites (arrows) are seen in this low power view. Scale bar 200 µm. INSERT. Long Htau neurite. Scale bar 10 µm. B. Same subject as A with a frontal Htau neurite counterstained with H. Scale bar 10 µm. INSERT. A frontal neuron with a Htau tangle. Scale bar 10 µm. C. Frontal section same 18 y APOE 3/4 with a tau plaque and a frontal neuron with a strong positive Htau nucleus. Scale bar 20 µm. D. Seventeen year old male, APOE 3/3, suicide, Htau neurite in substantia nigrae. Scale bar 10 µm. E. Same subject as D, higher power of substantia nigrae neurons showing strong nuclear Htau positivity (arrow). Scale bar 10 µm. F. Same subject as D and E, hippocampus section. Extensive nuclear Htau positivity of CA1 neurons. Scale bar 50 µm. INSERT. Close-up CA1 neuron and adjacent glial cell with strong nuclear Htau positivity. Scale bar 10 µm. G. Thirteen year old female, lower medulla. One Htau positive tangle at the medial longitudinal fasciculus. Scale bar 10 µm. H. Same child as G. Section of upper pons. Large globose tangle. Scale bar 10 µm. I. Eighteen year old male, APOE 3/4 frontal section. Diffuse amyloid plaque (arrow). IHCx4G8. Scale bar 200 µm. J. Eleven year old boy APOE 3/3 frontal section. Extensive capillary and arteriole amyloid deposition. IHCx4G8. Scale bar 100 µm. K. Same boy as J, frontal section showing a combination of beta amyloid neuropil and intraneuronal deposition (arrow). IHCx4G8. Scale bar 10 µm. L. Same as J, K subject. Frontal section with perivascular beta amyloid accumulation. The lumen of the vessel is marked L). IHCx4G8. Scale bar 20 µm. M. Same subject as J, K, L in a section of the dentate gyrus. Extensive pericapillary amyloid accumulation. IHCx4G8. Scale bar 100 µm. N. The extensive pericapillary amyloid accumulation extends throughout the CA hippocampal regions (arrows). Scale bar 100 µm. O. CA1 hippocampal region Htau nuclear positive neurons. IHCxAT8. Scale bar 100 µm. INSERT. Temporal cortex shows isolated neurons with granular cytoplasmic Htau reactivity adjacent with nuclear positive neurons. P. Subiculum section stained for beta amyloid 4G8 is negative. IHCx4G8. Scale bar 10 µm. Q. Transentorrhinal section stained for beta amyloid 4G8 is strongly positive. IHCx4G8. Scale bar 10 µm. R. Clusters of Htau positive neurites (arrows) are adjacent to hippocampal CA1 neurons in this 12 year old APOE 3/3 girl.INSERT. A large Htau positive material is seen in CA1 in the same child. Scale bar 10 µm. S. Higher power of choroid plexus from 11 year old to show the massive accumulation of beta amyloid and the presence of sub-epithelial calcifications in choroid plexus areas (C). IHCx4G8. Scale bar 10 µm. T. Eleven year old girl, APOE 3/3 temporal cortex. Significant accumulation of beta amyloid in endothelial cells (arrows) with deposition in adjacent neuropil. IHCx4G8. Scale bar 20 µm.

capacity of particles to exert both short and long term effects on the brain of exposed people around the world (Yarjanli et al., 2017; Alvarez et al., 2013).

The endotoxin tolerance-like state in SW Mexico City children is associated to the high amounts of lipopolysaccharides (LPS) in $PM_{2.5}$ and translates in a frontal significant upregulation of genes involved with downstream receptor signaling functions of the NOD-like receptors (Calderón-Garcidueñas et al., 2012). The issue is of significant interest in view of the 22 y old woman with no evidence of Htau pathology carried a TLR 4 Asp299Gly mutation, associated with endotoxin hyporesponsiveness causing interruption of the TLR4-mediated LPS signaling (Arbour et al., 2000). It is well known that TLRs play a key role

in the innate immune recognition of invading microorganisms, initiating proper immune responses, thus a subject carrying SNPs-Asp299gly and Thr399Ile-within the TLR4 gene will succumb to several infectious diseases but it will be protected against from atherosclerosis and AD. Fine and/or nanosize PM carrying lipopolysaccharides and entering the brain will fail to start an inflammatory cascade in the affected carriers.

This study has important suicide risk implications. In MMC, APOE4 carriers 25.2 ± 8.48 y-with accelerated NFT V and amyloid-β phase 3-, had the highest suicide risk, opening the possibility advanced Htau and amyloid stages contributed to depression and suicide at this early age. Relevant to suicide risk is Olfson et al. (2017) identifying APOE and IL6
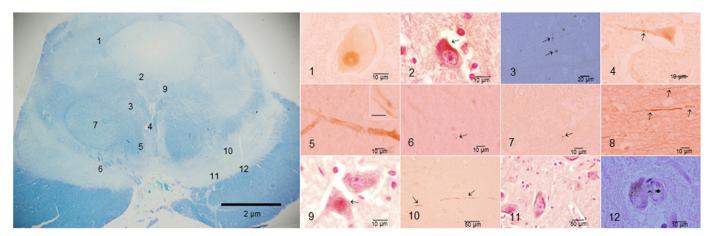
Fig. 8. Representative midbrain immunohistochemistry and H&E sections from subjects in the first and second decades of life. 1. Mesencephalic V neuron with + nuclear Htau in an 11 y old girl. AT8. Scale bar 10 μm. 2. Edinger-Westphal neuron with + cytoplasmic Htau (arrow) in a 17 y boy. Scale bar 10 μm. 3. Mesencephalic reticular formation + Htau neurite (upper arrow) and a + nucleus (lower arrow) in an 11 month old baby. Scale bar 20 μm. 4. Raphe neuron with cytoplasmic + Htau (arrow), in a 3 year old male. Scale bar 10 μm. 5. Blood vessels with + cytoplasmic + Htau in 2 y old male. Scale bar 10 μm. Insert, capillary in same region with cytoplasmic endothelial + Htau. Scale bar 10 μm. 6. Two year old male with a + Htau neurite (arrow) in substantia nigrae region. Scale bar 10 μm. 7. Eleven year old girl with a + Htau neurite in medial lemniscus (arrow). Scale bar 10 μm 8. Three year old male commissure of superior colliculus with + Htau fibers (arrows). Scale bar 10 μm 9. Seventeen year old male neurons of the III cranial nerve with + nuclear Htau (arrow) in contrast with the upper Htau negative neuron. Scale bar 10 μm. 10. One long + Htau neurite in the substantia nigrae of an 11 year old girl. Scale bar 50 μm. 11. Several neurites Htau + in substantia nigrae neurons in a 17 y old male. Htau + H Scale bar 50 μm. 12. Eleven year old male with loss of neuromelanin in a substantia nigrae. A macrophage (arrow head) with abundant neuromelanin is seen between the neuron and the blood vessel (*). H&E stain. Scale bar 10 μm.

as the top overall biomarkers of interest, both very significant in MMC children, along with brisk neuroinflammation (Calderón-Garcidueñas et al., 2008, 2016a, 2012).

In interpreting these findings, several limitations apply. First, in the selected age group, there is an overrepresentation of males, thus we are unable to discuss how the disease progresses in females. Second, since we had no means of assessing the subjects neurological, cognitive and imaging data, the direct association with Htau and amyloid stages is not possible. Third, the researchers did not have access to private information including medical records and/or occupation. This lack may

have led to relevant psychiatric,behavioral, and neurotoxic exposures information.

AD evolving from childhood is threating the wellbeing of our children and future generations. Pollution control should be prioritised, and identifying air pollution components for neural risk trajectories ought to be a priority in our prevention efforts to stop the disease.

A key challenge is to define clinical, laboratory, imaging, and cognitive *non-invasive* markers for the initial stages of the disease knowing Htau is the prime actor, the disease starts in the brainstem, and APOE4 carriers are at highest risk. It is imperative that we understand the
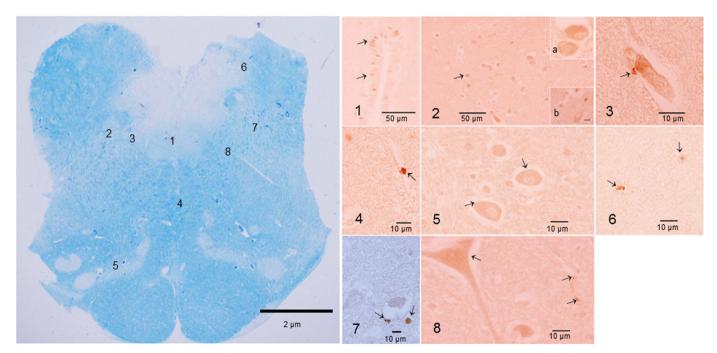

Fig. 9. Section from lower medulla in an 11 month old baby from a high PM$_{2.5}$ industrial area in the Mexico State. 1. Ependymal cells around show positive nuclear Htau (arrows). IHCxAT8. Scale bar 50 μm. 2. Lateral reticular formation neurons with + cytoplasmic Htau (arrows). Scale bar 50 μm INSERT a: higher power cytoplasmic + Htau in reticular neurons. INSERT b: Htau + neurite. 3. Medial reticular formation neuron with + Htau in hillock (arrow). Scale bar 10 μm. 4. Positive immunoreactive Htau structure adjacent to the wall of a blood vessel (arrow). Scale bar 10 μm. 5. Inferior olivary complex neurons with + cytoplasmic Htau (arrows). Scale bar 10 μm. 6. Immunoreactive Htau neurite (left arrow)and + nucleus (right arrow) in solitary tract. Scale bar 10 μm. 7. Lateral reticular formation neuron hillock with + Htau (left arrow) and an adjacent glial cell with nuclear + (right arrow). Scale bar 10 μm. 8. Medial reticular large neuron with + cytoplasmic Htau (left arrow) and a + Htau neurite (right arrows). Scale bar 10 μm.
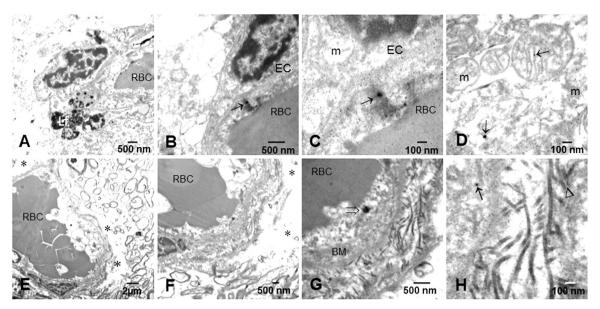
Fig. 10. Three year old male frontal (A–D) and temporal (E–H) electron microscopy sections. A. Frontal cortex blood vessel with abundant lipofuscin (Lf). Red blood cell in the lumen of the vessel is marked (RBC). Scale bar 500 nm. B. The endothelial cells tight junction is ill-defined and occupied by nanoparticles (arrow). Scale bar 500 nm. C. Higher power of B to show the combustion-derived nanoparticles 60 nm (arrow) in the tight junction. Scale bar 100 nm. D. High power of endothelial cell mitochondria shows the presence of nanoparticles within the mitochondrial matrix (upper arrow) and a 40 nm NP free in the cytoplasm (lower arrow). Scale bar 100 nm. E. Temporal white matter section. A small blood vessel shows an enlarged Virchow-Robin space (*). Scale bar 2 μm. F. Higher power of the same vessel to show the abnormal V-R space (*) and the RBC in the lumen. Scale bar 500 nm. G. Higher power, same vessel to show an angular euhedral 220 nm particle [Fig. 1C, D⁵](arrow head). Basement membranes are marked BM. Scale bar 500 nm. H. High power of a section of the same vessel to show isolated beta pleaded sheet helicoidal conformation fibers (head arrow) in the cytoplasm of the pericyte, between the endothelial and the pericyte BMs. One CDNP 28 nm in diameter is also seen (long arrow). Scale bar 100 nm.
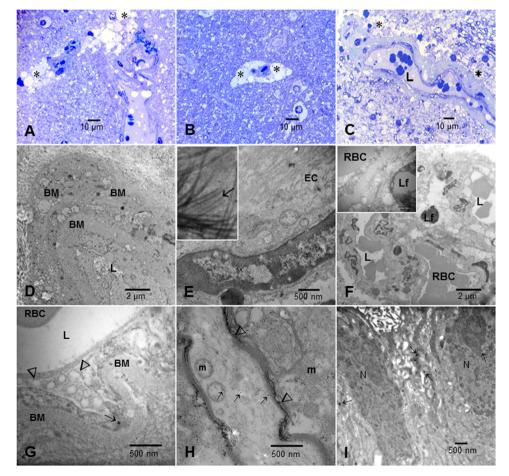

Fig. 11. Representative 1st and 2nd decades of life 1 μm toluidine blue and electron micrographs pictures. A. Fourteen year old girl section of frontal white matter. There is a significant expanded Virchow-Robin space with numerous lipid droplets (*). Scale bar 10 μm. B. Same 14 year old, section of frontal gray matter. A small arteriole with a large Virchow-Robin space occupied by lipid material (*). Scale bar 10 μm. C. Olfactory bulb in same girl. Vascular changes in this location are characterized by thickened walls, the Virchow-Robin space is occupied by cell debri (*). Scale bar 10 μm. D. Multiple basement membrane abnormal layers (BM) are seen in this olfactory bulb vessel. Scale bar 2 μm. E. Fourth teen year old girl with beta pleaded sheet helicoidal conformation fibers in the cytoplasm of an endothelial cell (EC). Numerous CDNPs are seen in the EC nucleus. Insert. Higher power of beta pleaded fibers. Scale bar 500 nm. F. Seventeen year old male APOE 3/3 with olfactory bulb blood vessels with numerous lipofuscin granules (Lf). INSERT. Higher power of Lf in pericytes. L is marking lumen of vessels with red blood cells (RBC). Scale bar 10 μm. G. Same child as F. High caveolar activity in endothelial cells, CDNPs in endothelial cells (arrow). Thickened basement membranes (BM). L is marking lumen of vessels with red blood cells (RBC). Scale bar 500 nm. H. Eleven month old baby frontal white matter with extensive deposition of CDNPs (arrows) in a myelinated axon. Nanoparticles are also seen inside abnormal mitochondria (m). Fragmented myelin is seen (arrow heads). Scale bar 500 nm. I. Choroid plexus in a 12 year old. CDNPs are numerous (arrows) and distributed through the cytoplasm and nucleus (N). The CP cilia are towards the upper portion of the picture. Scale bar 500 nm.
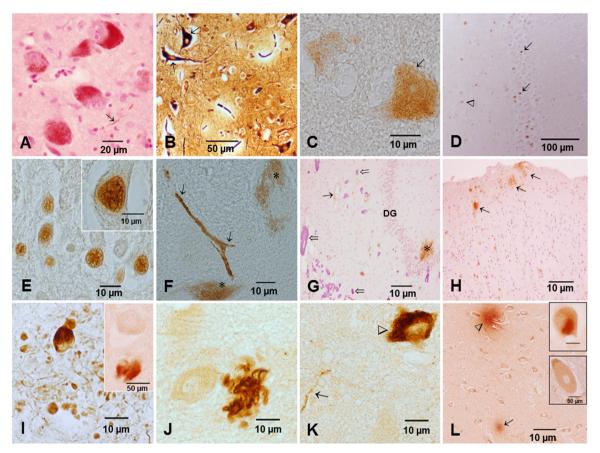
Fig. 12. Representative 3rd and 4th decades of life immunohistochemistry and modified Bielschowsky's silver sections. A. Thirty seven year old female, APOE 3/3 upper pons. Locus coeruleus neurons + Htau neurites (arrows). Scale bar 20 µm. B. Twenty eight year old female frontal cortex with Bielschowsky's neurofibrillary tangles (NFT) in pyramidal neurons (arrows). Scale bar 50 µm. C. Twenty-seven year old male, APOE 3/4, frontal cortex pyramidal neurons with + Htau (arrow). Scale bar 10 µm. D. Twenty-seven year old male, APOE 3/3 dentate gyrus + nuclear + Htau (arrows), + nuclei are also seen in the CA4 region (arrow head). Scale bar 100 µm. E. Same 27 y old from D in higher power dentate gyrus nuclear + Htau. INSERT. + nuclear Htau. Scale bar 10 µm. F. Forty year old male substantia nigrae + Htau neurons (*) and neurites (arrows). Scale bar 10 µm. G. Twenty-seven year old male, hippocampus 4G8 amyloid plaques (*) in dentate gyrus (DG), blood vessel walls (arrows) and extensive calcified blood vessels (open arrows). Scale bar 10 µm. H. Same 27 y old male as G, entorhinal cortex with extensive deposits of amyloid-β plaques (arrows). Scale bar 10 µm. I. Thirty-six year old male, APOE 3/4, frontal cortex, + Htau with numerous dystrophic neurites. Scale bar 10 µm. Insert: same subject temporal cortex neuron with + Htau adjacent to a negative neuron. Scale bar 50 µm. J. Forty year old male, midbrain section. Htau tangles abundant throughout. Scale bar 10 µm. K. Same subject as J. Tangles and neurites (arrow) in substantia nigrae. Scale bar 10 µm. L. Thirty-five year old male, temporal cortex with diffuse (arrow) and mature plaques (arrow head) and blood vessel amyloid deposits. Scale bar 10 µm INSERT: same subject neurons with abundant cytoplasmic 4G8 product. Scale bar 50 µm.

neural circuitry associated with the earliest cognitive and behavioral manifestations of AD.

Early interventions should be integrated in health and educational agendas along with identifying early gender-specific risk trajectories. We are certain air pollution should be included as an early risk factor in the research priorities to reduce global burden of dementia and the concept of preclinical AD ought to be revised. Finally, we urgently need to define paediatric environmental, nutritional, metabolic and genetic risk factor interactions of paramount importance to prevent a dreadful disease killing millions of people across the world.

Contributors

LCG had access to all the data in the study, in charge of the study concept and design, oversaw the project, took part in the collection of the data, cut the brainstems, did the immunohistochemistry, review the electron micrographs, staged all cases, draft the manuscript and wrote the final manuscript. She takes responsibility for the integrity of the data and the accuracy of the data analysis. AGM and RRR did the electron microscopy job, participated in acquisition, analysis and interpretation of data. RDC review the electron micrographs, staged all cases, and wrote the final manuscript. PSM provided advice on the protocol, performed all the statistical analysis, and wrote the final manuscript. RTJ analyzed the pollutant data, made air pollution figures

and wrote the pollution sections. RK, RDC, JAR and RVR participated in interpretation of data, drafting of the manuscript, wrote the final manuscript and provided critical revisions for important intellectual content.

Declaration of interests

Funding

Appendix A. Supplementary material

Supplementary data associated with this article can be found in the online version at http://dx.doi.org/10.1016/j.envres.2018.03.023.

References

Aiken, A.C., Salcedo, D., Cubison, M.J., et al., 2009. Mexico City aerosol analysis during MILAGRO using high resolution aerosol mass spectrometry at the urban supersite (T0) – Part 1: fine particle composition and organic source apportionment. Atmos. Chem. Phys. 9, 6633–6653.

Alvarez, Y.D., Fauerbach, J.A., Pellegrotti, J.V., et al., 2013. Influence of gold nano-particles on the kinetics of α-synuclein aggregation. Nano Lett. 13, 6156–6163.

Arbour, N.C., Lorenz, E., Schutte, B.C., et al., 2000. TLR4 mutations are associated with endotoxin hyporesponsiveness in humans. Nat. Genet. 25, 187–191.

Braak, H., Del Tredeci, K., 2015. The preclinical phase of the pathological process underlying sporadic Alzheimer's disease. Brain 138, 2814–2833.

Braak, H., Del Tredici, K., 2011. The pathological process underlying Alzheimer's disease in individuals under thirty. Acta Neuropathol. 121, 171–181.

Braak, H., Thal, D.R., Ghebremedhin, E., Del Tredeci, K., 2011. Stages of the pathological process in Alzheimer disease: age categories from 1 to 100 years. J. Neuropathol. Exp. Neurol. 70, 960–969.

Bravo-Alvarez, H.R., Torres-Jardón, R.J., 2002. Air pollution levels and trends in the Mexico City metropolitan area. In: Fenn, M., Bauer, L., Hernández, T. (Eds.), Urban Air Pollution and Forests: Resources at Risk in the Mexico City Air Basin Ecological Studies. Springer-Verlag, New York, pp. 121–159.

Calderón-Garcidueñas, L., Azzarelli, B., Acuna, H., et al., 2002. Air pollution and brain damage. Toxicol. Pathol. 30, 373–389.

Calderón-Garcidueñas, L., Solt, A.C., Henríquez-Roldán, C., et al., 2008. Long-term air pollution exposure is associated with neuroinflammation, an altered innate immune response, disruption of the blood-brain-barrier, ultrafine particulate deposition, and accumulation of amyloid beta-42 and alpha-synuclein in children and young adults. Toxicol. Pathol. 36, 289–310.

Calderón-Garcidueñas, L., Franco-Lira, M., Henríquez-Roldán, C., et al., 2010. Urban air pollution: influences on olfactory function and pathology in exposed children and young adults. Exp. Toxicol. Pathol. 62, 91–102.

Calderón-Garcidueñas, L., Engle, R., Mora-Tiscareño, A., et al., 2011a. Exposure to severe urban pollution influences cognitive outcomes, brain volume and systemic inflammation in clinically healthy children. Brain Cogn. 77, 345–355.

Calderón-Garcidueñas, L., D'Angiulli, A., Kulesza, R.J., et al., 2011b. Air pollution is associated with brainstem auditory nuclei pathology and delayed brainstem auditory evoked potentials. Int. J. Dev. Neurosci. 29, 365–375.

Calderón-Garcidueñas, L., Kavanaugh, M., Block, M., et al., 2012. Neuroinflammation, hyperphosphorylated tau, diffuse amyloid plaques, and down-regulation of the cellular prion protein in air pollution exposed children and young adults. J. Alzheimer Dis. 28, 93–107.

Calderón-Garcidueñas, L., Mora-Tiscareño, A., Franco-Lira, M., et al., 2015a. Decreases in short term memory, IQ and altered brain metabolic ratios in urban apolipoprotein ε4 children exposed to air pollution. APOE modulates children's brain air pollution responses. J. Alzheimer Dis. 45, 757–770.

Calderón-Garcidueñas, L., Mora-Tiscareño, A., Melo-Sánchez, G., et al., 2015b. A critical Proton MR Spectroscopy marker of Alzheimer's disease early neurodegenerative change: low hippocampal NAA/Cr ratio impacts APOE ε4 Mexico City children and their parents. J. Alzheimers Dis. 48, 1065–1075.

Calderón-Garcidueñas, L., Jewells, V., Galaz-Montoya, C., et al., 2016a. Interactive and additive influences of gender, BMI and Apolipoprotein 4 on cognition in children chronically exposed to high concentrations of PM$_{2.5}$ and ozone. APOE4 females are at highest risk in Mexico City. Environ. Res. 150, 411–422.

Calderón-Garcidueñas, L., Reynoso-Robles, R., Vargas-Martínez, J., et al., 2016b. Prefrontal White matter pathology in air pollution exposed Mexico City Young urbanites and their potential impact on neurovascular unit dysfunction and the development of Alzheimer's disease. Environ. Res. 146, 404–417.

Calderón-Garcidueñas, L., Ávila-Ramírez, J., Calderón-Garcidueñas, A., et al., 2016c. Cerebrospinal fluid biomarkers in highly exposed PM$_{2.5}$ urbanites: the risk of Alzheimer's and Parkinson's diseases in young Mexico city residents. J. Alzheimers Dis. 54, 597–613.

Calderón-Garcidueñas, L., Reynoso-Robles, R., Pérez-Guillé, B., et al., 2017. Combustion-derived nanoparticles, the neuroenteric system, cervical vagus, hyperphosphorilated alpha synuclein and tau in young Mexico City residents. Environ. Res. 159, 186–201.

Chen, H., Kwong, J.C., Copes, R., et al., 2017. Living near major roads and the incidence of dementia, Parkinson's disease, and multiple sclerosis: a population-based cohort study. Lancet 389, 718–726.

González-Maciel, A., Reynoso-Robles, R., Torres-Jardón, R., et al., 2017. Combustion-derived nanoparticles in key brain target cells and organelles in young urbanites: culprit hidden in plain sight in Alzheimer's disease development. J. Alzheimers Dis. 59, 189–208.

Iadecola, C., 2017. The neurovascular unit coming of age: a journey through neurovascular coupling in health and disease. Neuron 96, 17–42.

Jung, C.R., Lin, Y.T., Hwang, B., 2015. Ozone, particulate matter, and newly diagnosed Alzheimer's disease: a population-based cohort study in Taiwan. J. Alzheimers Dis. 44, 573–584.

Kicinski, M., Vermeir, G., Van Larebeke, N., et al., 2015. Neurobehavioral performance in adolescents is inversely associated with traffic exposure. Environ. Int. 75, 136–143.

Kovacs, G.G., 2017. Tauopathies. Handb. Clin. Neurol. 145, 355–368.

Maher, B., Ahmed, I.A.M., Karloukovski, V., et al., 2016. Magnetite pollution nanoparticles in the human brain. Proc. Natl. Acad. Sci. USA 113, 10797–10801.

Marr, L.C., Dzepina, K., Jimenez, J.L., et al., 2006. Sources and transformations of particle-bound polycyclic aromatic hydrocarbons in Mexico City. Atmos. Chem. Phys. 6, 1733–1745.

Molina, L.T., Madronich, S., Gaffney, J.S., et al., 2010. An overview of the MILAGRO 2006 Campaign: Mexico City emissions and their transport and transformation. Atmos. Chem. Phys. 10, 8697–8760.

Olfson, M., Blanco, C., Wall, M., et al., 2017. National trends in suicide attempts among adults in the United States. JAMA Psychiatry 74, 1095–1103.

Querol, X., Pey, J., Minguillón, M.C., et al., 2008. PM speciation and sources in Mexico during the MILAGRO-2006 Campaign. Atmos. Chem. Phys. 8, 111–121.

Rüb, U., Stratmann, K., Heinsen, H., et al., 2016. The brainstem tau cytoskeletal pathology of Alzheimer's disease: a brief historical overview and description of its anatomical distribution pattern, evolutional features, pathogenetic and clinical relevance. Curr. Alzheimer Res. 13, 1178–1197.

Secretaría del Medio Ambiente del Distrito Federal: ⟨http://www.aire.df.gob.mx⟩, (Accessed 9 November 2017).

SEDEMA, 2017. Secretaría del Medio Ambiente Ciudad de México. Estadísticas. Accessed on October 2017 at: ⟨http://www.aire.cdmx.gob.mx/default.php⟩.

Sperling, R.A., Aisen, P.S., Beckett, L.A., et al., 2011. Toward defining the preclinical stages of Alzheimer's disease: recommendations from the National Institute on Aging-Alzheimer's Association workgroups on diagnostic guidelines for Alzheimer's disease. Alzheimers Dement. 7, 280–292.

Sultan, A., Nesslany, F., Violet, M., et al., 2011. Nuclear tau, a key player in neuronal DNA protection. J. Biol. Chem. 286, 4566–4575.

Thal, D.R., Rüb, U., Orantes, M., Braak, H., 2002. Phases of A beta-deposition in the human brain and its relevance for the development of AD. Neurology 58, 1791–1800.

Vega, E., Eidels, S., Ruiz, H., et al., 2010. Particulate air pollution in Mexico City: a detailed view. Aerosol Air Qual. Res. 10, 193–211.

Yarjanli, Z., Ghaedi, K., Esmaeili, A., et al., 2017. Iron oxide nanoparticles may damage to the neural tissue through iron accumulation, oxidative stress, and protein aggregation. BMC Neurosci. 18, 51.

Zecca, L., Tampellini, D., Gerlach, M., et al., 1969. Substantia Nigra neuromelanin: structure, synthesis, and molecular behavior. J. Neuropathol. Exp. Neurol. 28, 419–441.